ELSEVIER

Infrared Physics & Technology 43 (2002) 187–210

INFRARED PHYSICS & TECHNOLOGY

www.elsevier.com/locate/infrared

Infrared detectors: an overview

Antoni Rogalski *

Institute of Applied Physics, Military University of Technology, 2 Kaliskiego St., 00-908 Warsaw 49, Poland

Abstract

The paper presents progress in infrared (IR) detector technologies during 200 history of their development. Classification of two types of IR detectors (photon detectors and thermal detectors) is done on the basis of their principle of operation. The overview of IR systems and detectors is presented. Also recent progress in different IR technologies is described. Discussion is focused mainly on current and the most rapidly developing detectors: HgCdTe heterostructure photodiodes, quantum well AlGaAs/GaAs photoresistors, and thermal detectors. The outlook for near-future trends in IR technologies is also presented.

Keywords: Photon detectors; Thermal detectors; Focal plane arrays; Two-colour detectors

1. Introduction

Looking back over the past 1000 years we notice that infrared (IR) radiation itself was unknown until 200 years ago when Herschel's experiment with thermometer was first reported. He built a crude monochromator that used a thermometer as a detector so that he could measure the distribution of energy in sunlight. In April 1800 he wrote [1]: *Thermometer No. 1 rose 7 degrees in 10 minutes by an exposure to the full red coloured rays. I drew back the stand... thermometer No. 1 rose, in 16 minutes,* $8\frac{3}{8}$ *degrees when its centre was* $1/2$ *inch out of the visible rays.*

The early history of IR was reviewed about 40 years ago in two well-known monographs [2,3]. The most important steps in development of IR detectors are the following:

- in 1921 Seebeck discovered the thermoelectric effect and soon thereafter demonstrated the first thermocouple,
- in 1829 Nobili constructed the first thermopile by connecting a number of thermocouples in series [4],
- in 1933 Melloni modified thermocouple design and used bismuth and antimony for it [5].

Langley's bolometer appeared in 1880 [6]. Langley used two thin ribbons of platinum foil, connected so as to form two arms of a Wheatstone bridge. Langley continued to develop his bolometer for the next 20 years (400 times more sensitive than his first efforts). His latest bolometer could detect the heat from a cow at a distance of a quarter of mile. Thus, at the beginning the development of IR detectors was connected with thermal detectors.

The photon detectors were developed in XX century. The first IR photoconductor was developed by Case in 1917 [7]. In 1933 Kutzscher at

* Fax: +48-22-685-9109.
E-mail address: rogan@wat.waw.pl (A. Rogalski).

1350-4495/02/$ - see front matter
PII: S1350-4495(02)00140-8

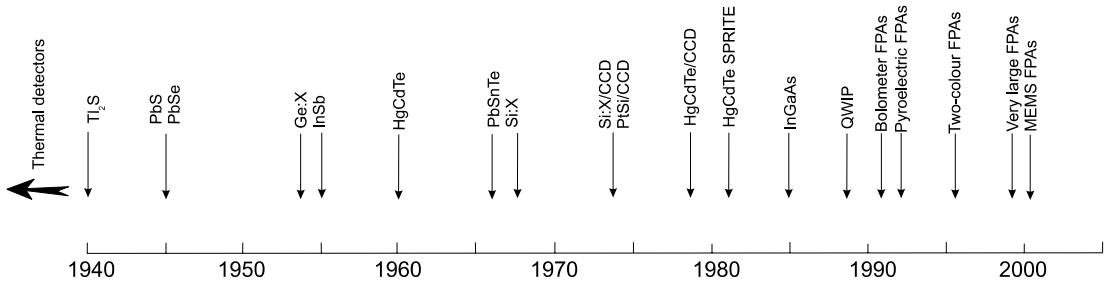

Fig. 1. History of the development of IR detectors.

University of Berlin, discovered that lead sulphide (from natural galena found in Sardinia) was photoconductive and had response to about 3 μm [8].

Many materials have been investigated in the IR field. Observing a history of the development of the IR detector technology, a simple theorem, after Norton [9], can be stated: *All physical phenomena in the range of about 0.1–1 eV can be proposed for IR detectors*. Among these effects are: thermoelectric power (thermocouples), change in electrical conductivity (bolometers), gas expansion (Golay cell), pyroelectricity (pyroelectric detectors), photon drag, Josephson effect (Josephson junctions, SQUIDs), internal emission (PtSi Schottky barriers), fundamental absorption (intrinsic photodetectors), impurity absorption (extrinsic photodetectors), low-dimensional solids (superlattice (SL) and quantum well (QW) detectors), different type of phase transitions, etc.

Fig. 1 gives approximate dates of significant development efforts for the materials mentioned. The years during World War II saw the origins of modern IR detector technology. Interest has centred mainly on the wavelengths of the two atmospheric windows 3–5 and 8–14 μm, though in recent years there has been increasing interest in longer wavelengths stimulated by space applications [10].

2. Classification of IR detectors

Progress in IR detector technology is connected mainly to semiconductor IR detectors, which are included in the class of photon detectors. In this class of detectors the radiation is absorbed within the material by interaction with electrons. The observed electrical output signal results from the changed electronic energy distribution. The photon detectors show a selective wavelength dependence of the response per unit incident radiation power. They exhibit both perfect signal-to-noise performance and a very fast response. But to achieve this, the photon detectors require cryogenic cooling. Cooling requirements are the main obstacle to the more widespread use of IR systems based on semiconductor photodetectors making them bulky, heavy, expensive and inconvenient to use. Depending on the nature of interaction, the class of photon detectors is further sub-divided into different types. The most important are: intrinsic detectors, extrinsic detectors, photoemissive (metal silicide Schottky barriers) detectors, and quantum well detectors. Table 1 shows the comparison of various IR detectors.

The second class of IR detectors is composed of thermal detectors. In a thermal detector the incident radiation is absorbed to change temperature of the material, and the resultant change in some physical properties is used to generate an electrical output. The detector element is suspended on lags, which are connected to the heat sink. Thermal effects are generally wavelength independent; the signal depends upon the radiant power (or its rate of change) but not upon its spectral content. In pyroelectric detectors a change in the internal spontaneous polarisation is measured, whereas in the case of bolometers a change in the electrical resistance is measured. In contrast to photon detectors, the thermal detectors typically operate at room temperature. They are usually characterized

Table 1
Comparison of IR detectors (after Ref. [11])

Detector type	Advantages	Disadvantages
Thermal	Light, rugged, reliable, and low cost Room temperature operation	Low detectivity at high frequency Slow response (ms order)
Photon		
Intrinsic		
IV–VI	Available low-gap materials Well studied	Poor mechanical Large permittivity
II–VI	Easy band-gap tailoring Well-developed theory and exp. Multicolour detectors	Non-uniformity over large area High cost in growth and processing
III–V	Good material and dopants Advanced technology Possible monolithic integration	Heteroepitaxy with large lattice mismatch
Extrinsic	Very long wavelength operation Relatively simple technology	Extremely low temperature operation
Free carriers	Low-cost, high yields Large and close packed 2D arrays	Low quantum efficiency Low temperature operation
Quantum wells		
Type I	Matured material growth Good uniformity over large area Multicolour detectors	Low quantum efficiency Complicated design and growth
Type II	Low Auger recombination rate Easy wavelength control	Complicated design and growth Sensitive to the interfaces

by modest sensitivity and slow response but they are cheap and easy to use. The greatest utility in IR technology has found bolometers, pyroelectric detectors and thermopiles.

Up till the nineties, thermal detectors have been considerably less exploited in commercial and military systems in comparison with photon detectors. The reason for this disparity is that thermal detectors are popularly believed to be rather slow and insensitive in comparison with photon detectors. As a result, the worldwide effort to develop thermal detectors was extremely small relative to that of photon detector. In the last decade however, it has been shown that extremely good imagery can be obtained from large thermal detector arrays operating uncooled at TV frame rates. The speed of thermal detectors is quite adequate for non-scanned imagers with two-dimensional (2D) detectors. The moderate sensitivity of thermal detectors can be compensated by a large number of elements in 2D electronically scanned arrays. With large arrays of thermal detectors the best values of NEDT, below 0.1 K, could be reached because effective noise bandwidths < 100 Hz can be achieved.

Uncooled, monolithic focal plane arrays (FPAs) fabricated from thermal detectors may revolutionise development of thermal imagers. Recently, very encouraging results have been obtained with micromachined silicon bolometer [10,12] and pyroelectric detector arrays [10,13].

3. Focal plane arrays

There are a number of architectures used in the development of IR FPAs. In general, they may be classified as hybrid and monolithic. The central design questions involve performance advantages versus ultimate producibility. Each application may favour a different approach depending on the technical requirements, projected costs, and schedule.

In the monolithic approach, some of the multiplexing is done in the detector material itself than in an external readout circuit. The basic element of a monolithic array is a metal–insulator–semiconductor (MIS) structure as shown in Fig. 2(c). A MIS capacitor detects and integrates the IR-generated photocurrent. Although efforts have been made to develop monolithic FPAs using narrow-gap semiconductors, silicon-based FPA technology with Schottky-barrier detectors is the only technology, which has matured to a level of practical use.

Hybrid FPAs detectors and multiplexers are fabricated on different substrates and mated with each other by the flip-chip bonding (Fig. 3) or loophole interconnection. In this case we can optimise the detector material and multiplexer independently. Other advantages of the hybrid FPAs

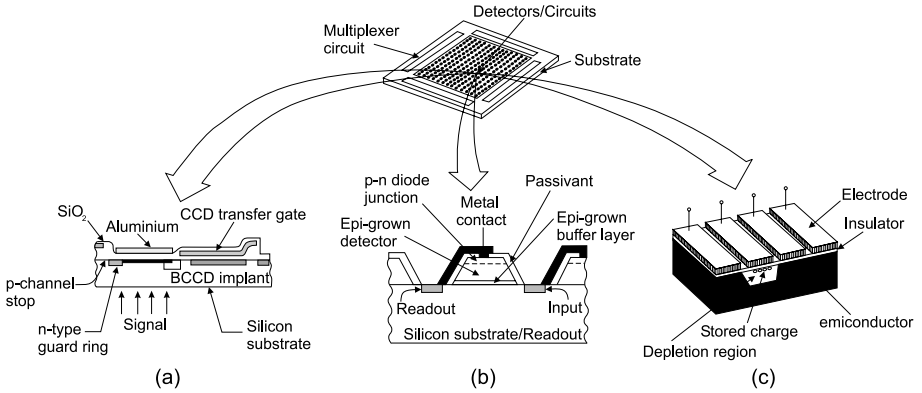

Fig. 2. Monolithic IR FPAs: (a) all-silicon; (b) heteroepitaxy-on-silicon; (c) non-silicon (e.g., HgCdTe CCD) (after Ref. [14]).

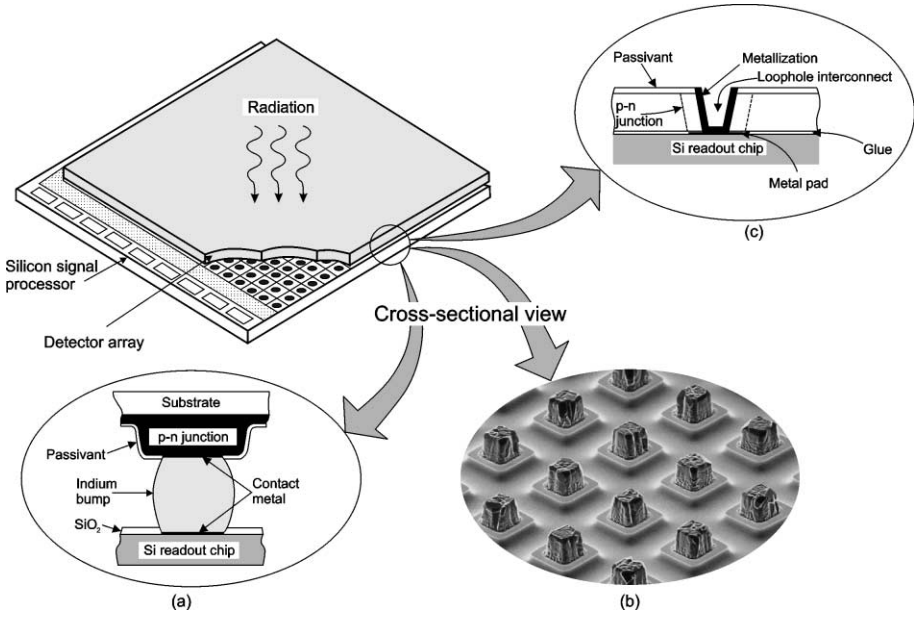

Fig. 3. Hybrid IR FPA with independently optimised signal detection and readout: (a) indium bump technique, (b) loophole technique.

are near 100% fill factor and increased signal-processing area on the multiplexer chip. In the flip-chip bonding, the detector array is typically connected by pressure contacts via indium bumps to the silicon multiplex pads. The detector array can be illuminated from either the frontside or backside (with photons passing through the transparent detector array substrate). In general, the latter approach is most advantageous. In HgCdTe hybrid FPAs, photovoltaic detectors are formed on thin HgCdTe epitaxial layer on transparent CdTe or CdZnTe substrates. For HgCdTe flip-chip hybrid technology, the maximum chip size is of the order of 10 mm square. In order to overcome this problem, the technology is being developed with sapphire or silicon as the substrate of HgCdTe detectors. When using opaque materials, substrates must be thinned to 10–20 μm in order to obtain sufficient quantum efficiencies and reduce the crosstalk.

There is a large research activity directed towards 2D staring arrays detectors consisting of more than 10^6 elements. IR FPAs have nominally the same growth rate as dynamic random access memory (RAM) integrated circuits (ICs) (it is consequence of Moore's Law, which predicts the ability to double transistor integration on each IC about every 18 months) but lag behind in size by about 5–10 years. ROIC's are somewhat analogous to dynamic RAM—only readouts require a minimum of three transistors per pixel compared to one per memory cell. Consequently, whereas various 64×64 FPAs were available in the early 1980s, several vendors are now producing monolithic FPAs in the TV-compatible 1040×1040 formats. Fig. 4 illustrates the trend of array size over the past 25 years and some projections of what will evolve in the coming decade. Rockwell has developed the world's largest HgCdTe short wavelength IR (SWIR) FPA for astronomy and low-background applications. The format of the device is a hybrid 2048×2048 with a unit cell size of 18 μm × 18 μm. Table 2 contains description of representative IR FPAs that are commercially available as standard products and/or catalogue items from the major manufactures. Ten years ago, high quality single element detectors often were priced over $2000, but now, some current IR FPA production costs are less than $1 per detector and even greater reductions are expected in the near future.

Two types of silicon addressing circuits have been developed: CCDs and complementary metal-oxide-semiconductor (CMOS) switches. The photogenerated carriers are first integrated in the well formed by a photogate and subsequently transferred to slow (vertical) and fast (horizontal) CCD shift registers.

An attractive alternative to the CCD readout is coordinative addressing with CMOS switches. The

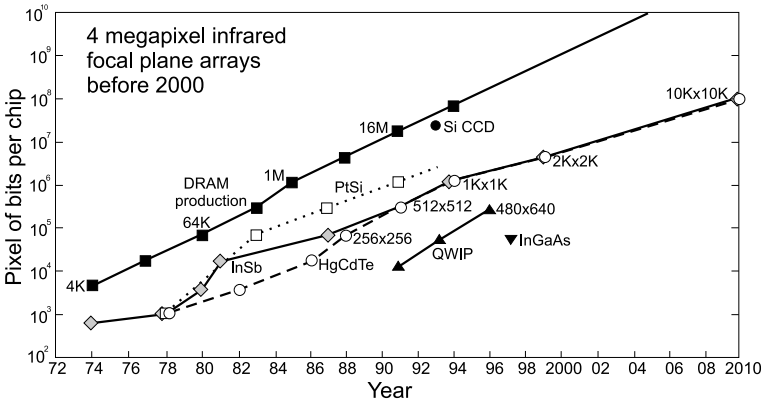

Fig. 4. Increase in array format size over the past 25 years and projections for the coming decade. PtSi, InSb, and HgCdTe have been following the pace of dynamic RAM, offset by about a decade. QWIP detectors have been recently reported in sizes as large as 640×480 pixels (after Ref. [15]).

Table 2
Representative IR FPAs offered by some major manufacturers

Manufacturer/web site	Size/architecture	Pixel size (μm)	Detector material	Spectral range (μm)	Operating temperature (K)	$D^*(\lambda_p)$ (cm $Hz^{1/2}$ W^{-1})/ NETD (mK)
Raytheon/	256 × 256/H	30 × 30	InSb	1–5.5	10–77	
www.raytheon.com	1024 × 1024/H	27 × 27	InSb	0.6–5.0	35	
	320 × 240/H	50 × 50	Si:As BIB	2–28	4–10	
	128 × 128/H	40 × 40	HgCdTe	9–11	80	
	256 × 256/H	30 × 30	HgCdTe	8.5–11	77–100	
	320 × 240/M	48 × 48	VO_x (bolometer)	8–14	300	50
	328 × 245/H	35 × 35	Pyro (BST)	8–14	300	>50
Rockwell/Boeing/	256 × 256/H	40 × 40	HgCdTe	>15	77	
www.boeing.com	640 × 480/H	27 × 27	HgCdTe	>10	77	
www.rsc.rockwell.com	225 × 256/H	40 × 40	HgCdTe	1–4.6	120	>10
	640 × 480/H	27 × 27	HgCdTe	1–4.6	120	>25
	2048 × 2048/H	18 × 18	HgCdTe	1–2.5	95–120	$> 1 \times 10^{14}$
	320 × 240/M	48 × 48	VO_x (bolometer)	8–14	300	50
Mitsubishi/www.mits-	256 × 256/M	52 × 40	PtSi	3–5	77	0.036
ubishi-imaging.com	512 × 512/M	26 × 20	PtSi	3–5	77	0.033
	1024 × 1024/M	17 × 17	PtSi	3–5	77	0.10
BAE Systems	256 × 256/H	30 × 30	HgCdTe	1–10	80	
	432 × 432/H		HgCdTe	1–5	80	
	640 × 480/M	28 × 28	VO_x (bolometer)	8–14	≈300	60
Sofradir/	128 × 128/H	50 × 50	HgCdTe	7.7–10	80	1.1×10^{11}/10
Infrared.sofradir.com	128 × 128/H	50 × 50	HgCdTe	3.7–4.8	90	4.3×10^{11}/7
	128 × 128/H	50 × 50	HgCdTe	2.5–4.2	195	7.5×10^{11}/36
	320 × 240/H	30 × 30	HgCdTe	3.7–4.8	120	1.0×10^{12}/8
	320 × 240/M	45 × 45	Amorphous Si (bolometer)	8–14	−20 to 60 °C	80
Sarnoff/	320 × 244/M	23 × 32	PtSi	1–5	77	
www.sarnoff.com	640 × 480/M	24 × 24	PtSi	1–5	77	
Eastman-Kodak/ www.kodak.com	486 × 640/M	25 × 25	PtSi	1–5	77	
Marconi/www.	128 × 128/H	50 × 50	HgCdTe	8–12	77	
gec-marconi.com/	384 × 288/H	30 × 30	HgCdTe	3–5	80	15
infra-red/	256 × 128/H	56 × 56	Pyro (PST)	8–14	≈300	90
	384 × 288/H	40 × 40	Pyro (PST)	8–14	≈300	130
AEG/www.aeg.com/	256 × 256/M	24 × 24	PtSi	3–5	77	75
e_produkte.htm	486 × 640/M	24 × 24	PtSi	3–5	77	70
	256 × 256/H	40 × 40	HgCdTe	8–10	80	20
	640 × 512/H	24 × 24	HgCdTe	3–5	80	20
	256 × 256/H	40 × 40	QWIP	8–10	60	10
	640 × 512/H	24 × 24	QWIP	8–10	60	20
JPL/www.jpl.nasa.gow	128 × 128/H	50 × 50	QWP	15 (λ_c)	45	30
	256 × 256/H	38 × 38	QWIP	9 (λ_c)	70	40
	640 × 486/H	18 × 18	QWIP	9 (λ_c)	70	36
Sensors Unlimited/	128 × 128/H	60 × 60	InGaAs	0.9–1.7	300	$>10^{13}$
www.sensorsinc.com	320 × 240/H	40 × 40	InGaAs	0.9–1.7	300	$>10^{12}$

H—hybrid, M—monolithic.

advantages of CMOS are that existing foundries. Design rules of 0.25 μm are in production with pre-production runs of the 0.18 μm design rules. At present, CMOS with minimum feature $\leqslant 0.5$ μm is also enabling monolithic visible CMOS imagers.

4. Viewpoint on IR detector technologies

During the past four decades mercury cadmium telluride (HgCdTe) has became the most important semiconductor for the middle and long wavelength ($\lambda = 3$–30 μm) IR photodetectors. The short wavelength region has been dominated by III–V compounds (InGaAs, InAsSb, InGaSb).

There have been numerous attempts to replace HgCdTe with alternative materials. At present, several other variable gap alloy systems are known including closely related mercury alloys HgZnTe, HgMnTe, lead tin tellurides and selenides, InAsSb, III–VI compounds with thallium and bismuth, free-carrier detectors and low-dimensional solids. The main motivations, behind the numerous attempts to replace HgCdTe, are technological problems of this material. One of them is weak Hg–Te bond, which results in bulk and surface and interface instabilities. Uniformity and yield are still issues. Nevertheless, HgCdTe remains the leading semiconductor for IR detectors. The most important reasons for this are:

- No one of the new materials offers fundamental advantages over HgCdTe. While the figure of merit, (α/G) (where α is the absorption coefficient and G is the thermal generation rate) [16], of various narrow-gap semiconductors seems to be very close to that of HgCdTe, the free-carrier detectors and GaAs/AlGaAs superlattice devices have several order of magnitude smaller α/G.
- HgCdTe exhibits extreme flexibility, it can be tailored for optimised detection at any region of IR spectrum, dual and multicolour devices can be easily constructed.
- The present development of IR photodetectors has been dominated by complex band-gap heterostructures. Among various variable band-gap semiconductor alloys, HgCdTe is the only one material covering the whole IR spectral range having nearly the same lattice parameter. The difference of lattice parameter between CdTe ($E_g = 1.5$ eV) and $Hg_{0.8}Cd_{0.2}Te$ ($E_g = 0.1$ eV) is $\approx 0.2\%$. Replacing small fraction of Cd with Zn or Te with Se can compensate the residual lattice mismatch. The independence of lattice parameter on composition is a major advantage of HgCdTe over any other materials.

Heterojunctions are helpful in achieving high performance in practice. For example, the narrow-gap HgCdTe that absorbs IR radiation can be buried encapsulated in wider gap HgCdTe preventing instabilities due to the weak Hg–Te bonds.

When background-photon noise is the dominant noise mechanism, the detector is operating in an ideal mode, and is said to exhibit background limited performance (BLIP). BLIP temperature is defined that the device is operating at a temperature at which the dark current equals the background photocurrent, given a field of view (FOV), and a background temperature. In Fig. 5, plots of the calculated temperature required for BLIP operation in 30° FOV, are shown as a function of cutoff wavelength. We can see that the operating temperature of "bulk" intrinsic IR detectors (HgCdTe and PbSnTe) is higher than for other types of photon detectors. HgCdTe detectors with

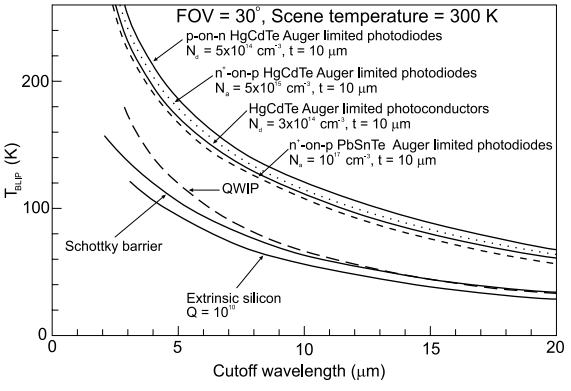

Fig. 5. Estimation of the temperature required for background limited operation of different types of photon detectors. For the calculations FOV = 30° and $T_B = 300$ K are assumed (after Ref. [17]).

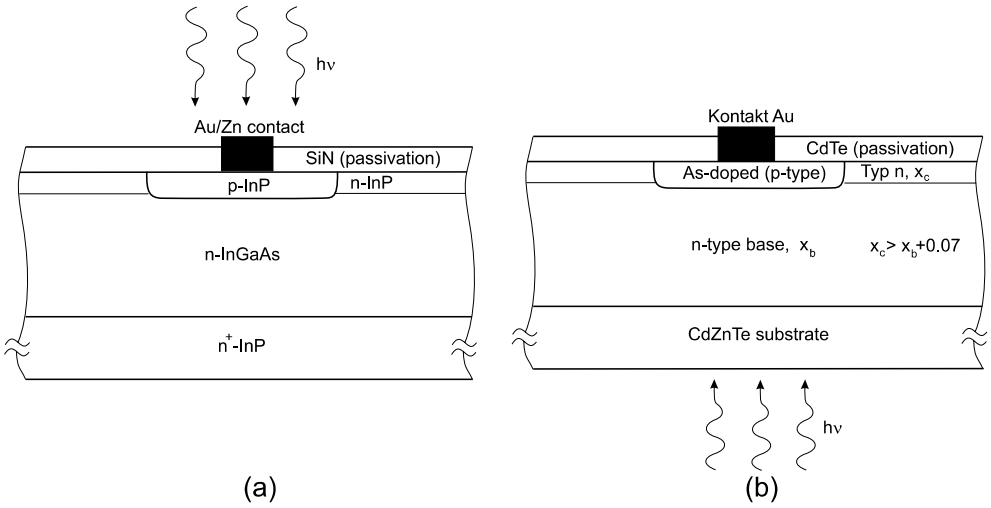

Fig. 6. Double layer planar heterostructure cross-section schematics for SWIR InGaAs (a) and HgCdTe (b) photodiodes.

BLIP operate with thermoelectric coolers in the MWIR range, but the LWIR detectors ($8 \leqslant \lambda_c \leqslant 12$ μm) operate at ≈100 K. HgCdTe photodiodes exhibit higher operating temperature compared to extrinsic detectors, silicide Schottky barriers and QWIPs. However, the cooling requirements for QWIPs with cutoff wavelengths below 10 μm are less stringent in comparison with extrinsic detectors and Schottky-barrier devices.

Recently, more interest has been focused on p–n junction heterostructure photodiodes. In comparison with heterostructures, homojunctions have a lower breakdown voltage and a large reverse leakage current. Another aspect of photodiode design is the required bandwidth for high-speed operation.

Photodiodes with their very low power dissipation, easy multiplexing on focal plane silicon chip and less stringent noise requirements for the readout devices and circuits, can be assembled in 2D arrays containing a very large number of elements, limited only by existing technologies.

Epitaxy is the preferable technique to obtain device-quality materials. Among the various epitaxial techniques, liquid phase epitaxy (LPE) is the most mature method. LPE growth must be carried out at relatively high growth temperature with adherent interdiffusion and resulting graded interfaces. Recent efforts are aimed mostly at low growth temperature techniques: metalorganic chemical vapour deposition (MOCVD) and molecular beam epitaxy (MBE).

The baseline detector architecture for SWIR InGaAs and HgCdTe is P^+-on-n device (symbol P denotes wider gap). Fig. 6 shows the double layer heterostructure (DLPH) device cross-sections for both types of photodiodes. Apart from the above described benefits, incorporation of a buried narrow-band-gap active layer in the DLPH reduces tunnelling currents and increases the total dose radiation hardness, both of which are essential detector attributes for remote sensing applications. The thickness of the base region should be optimised for near unity quantum efficiency and a low dark current. This is achieved with a base thickness (typically about 5–7 μm) slightly higher than the inverse absorption coefficient for single pass devices. Low doping is beneficial for a low thermal generation and high quantum efficiency. Since the diffusion length in absorbing region is typically longer than its thickness, any carriers generated in the base region can be collected giving rise to the photocurrent.

4.1. InGaAs photodiodes

The need for high-speed, low-noise $In_xGa_{1-x}As$ (InGaAs) photodetectors for use in lightwave

communication systems operating in the 1–1.7 μm wavelength region ($x = 0.53$) is well established. $In_{0.53}Ga_{0.47}As$ alloy is lattice matched to the InP substrate. Having lower dark current and noise than indirect-band-gap germanium, the competing near-IR material, the material is addressing both entrenched applications including low light level night vision and new applications such as remote sensing, eye-safe range finding and process control [18]. By changing the alloy composition of the InGaAs absorption layer, the photodetector responsivity can be maximized at the desired wavelength of the end user to enhance the signal-to-noise ratio.

InGaAs-detector processing technology is similar to that used with silicon, but the detector fabrication is different. The InGaAs detector's active material is deposited onto a substrate using chloride VPE or MOCVD techniques adjusted for thickness, background doping, and other requirements. Planar technology evolved from the older mesa technology and at present is widely used due to its simple structure and processing as well as the high reliability and low cost (see Fig. 6(a)).

Standard $In_{0.53}Ga_{0.47}As$ photodiodes have radiative-limited room temperature detectivity of $\sim 10^{13}$ cm $Hz^{1/2}$ W^{-1}. With increasing cutoff wavelength, detectivity decreases, what is shown in Fig. 7. The highest quality InGaAs photodiodes have been grown by MOCVD [19]. Their performance is comparable with HgCdTe photodiodes.

Linear array formats of 256, 512 and 1024 elements have been fabricated for environmental sensing from 0.8 to 2.6 μm. The size of pixels are different; from 30×30 μm^2 (with spacing of 50 μm), 25×500 μm^2 to 13×500 μm^2 (with spacing of 25 μm). Sensors Unlimited offers $10 \times 10 \times 6$ cm line-scan cameras incorporating linear InGaAs FPAs of up to 512 elements on a 50 μm pitch. A room temperature staring cameras are based on 128×128 and 320×240 InGaAs FPAs.

4.2. InSb photodiodes

InSb material is far more mature than HgCdTe and good quality more than 7 cm diameter bulk substrates are commercially available [20]. InSb

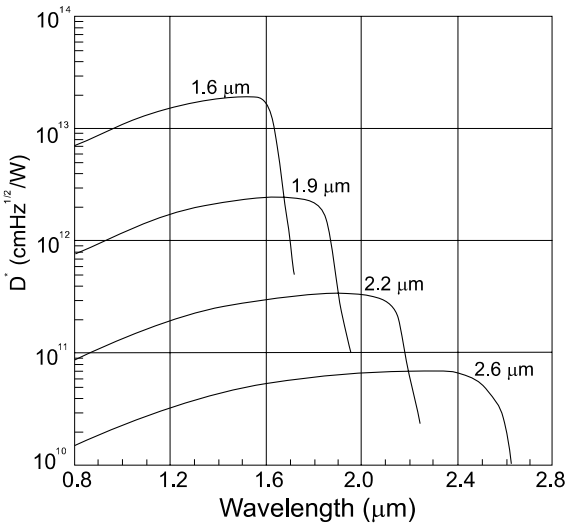

Fig. 7. Room temperature detectivity of InGaAs photodiodes with cutoff wavelength at 1.6, 1.9, 2.2, and 2.6 μm, respectively.

photodiodes have been available since the late fifties and they are generally fabricated by impurity diffusion and ion implantation. Epitaxy is not used; instead, the standard manufacturing technique begins with bulk n-type single crystal wafers with donor concentration about 10^{15} cm^{-3}. Wimmers et al. have presented the status of InSb photodiode technology for a wide variety of linear and FPAs [21,22].

Typical InSb photodiode RA product at 77 K is 2×10^6 Ω cm^2 at zero bias and 5×10^6 Ω cm^2 at slight reverse biases of approximately 100 mV. This characteristics is beneficial when the detector is used in the capacitive discharge mode. As element size decreases below 10^{-4} cm^{-2}, some slight degradation in resistance due to surface leakage occurs.

InSb photodiodes can also be operated in the temperature range above 77 K. Of course, the RA products degrade in this region. At 120 K, RA products of 10^4 Ω cm^2 are still achieved with slight reverse bias, making BLIP operation possible. The quantum efficiency in InSb photodiodes optimised for this temperature range remains unaffected up to 160 K. Detectivity increases with reduced background flux (narrow FOV and/or cold filtering) as illustrated in Fig. 8.

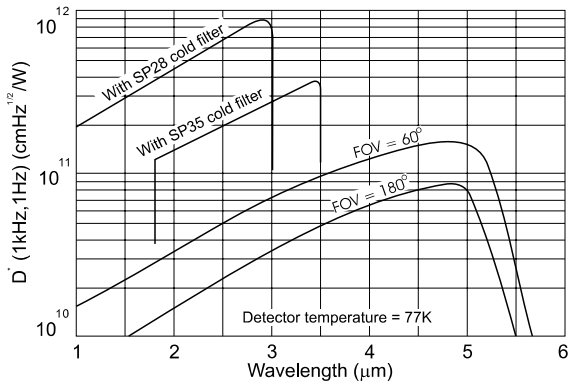

Fig. 8. Detectivity as a function of wavelength for an InSb photodiode operating at 77 K (after Judson, *Infrared Detectors* Catalog, 1999).

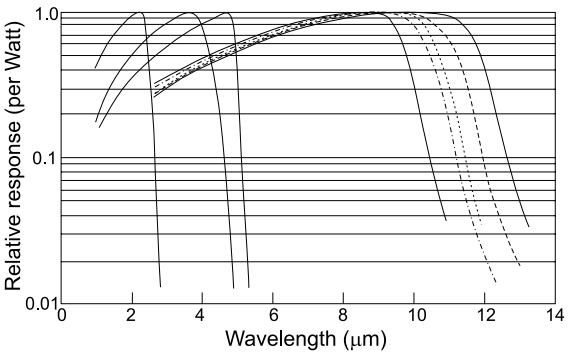

Fig. 9. Representative spectral response data for HgCdTe photodiodes.

InSb photovoltaic detectors are widely used for ground-based IR astronomy and for applications aboard the Space Infrared Telescope Facility. Recently, impressive progress has been made in the performance of InSb hybrid FPAs. An array size of 1024×1024 is possible because the InSb detector material is thinned to <10 μm (after surface passivation and hybridisation to a readout chip) which allows it to accommodate the InSb/silicon thermal mismatch [23]. Linear array formats of 64, 128 and 256 elements are also produced with frontside-illuminated detectors for both high-background and astronomy applications. Element sizes depend on device format and range from 20×20 to 200×200 μm.

The cryogenically cooled InSb and HgCdTe arrays have comparable array size and pixel yield at MWIR spectral band. However, wavelength tunability and high quantum efficiency have made HgCdTe the preferred material.

4.3. HgCdTe photodiodes

HgCdTe photodiodes are available to cover the spectral range from 1 to 20 μm. Fig. 9 illustrates representative spectral response from photodiodes. Spectral cutoff can be tailored by adjusting the HgCdTe alloy composition.

Epitaxial techniques are preferred technique to obtain device-quality HgCdTe material for IR devices. Epitaxial growth of the HgCdTe detector array on a Si substrate, rather than CdZnTe, has emerged as a particularly promising approach to scale up wafer dimensions and achieve a cost-effective production [24]. MBE offers unique capabilities in material and device engineering including the lowest growth temperature, superlattice growth and potential for the most sophisticated composition and doping profiles. The growth temperature is less than 200 °C for MBE but around 350 °C for MOCVD, making it more difficult to control the p-type doping in the MOCVD due to the formation of Hg vacancies.

Different HgCdTe photodiode architectures have been fabricated that are compatible with backside and frontside-illuminated hybrid FPA technology [18,25]. The fabrication of HgCdTe photodiodes was usually based on the most common n^+–p and P^+–n DLHJ structure. In these photodiodes the base p-type layers (or n-type layers) are sandwiched between CdZnTe substrate and high-doped (in n^+–p structures) or wider-gap (in P^+–n structure) regions. Due to backside illumination (through CdZnTe substrate) and internal electric fields (which are "blocking" for minority carriers), influence of surface recombinations on the photodiodes performance is eliminated. Both optical and thermal generations are suppressed in the n^+-region due to the Burstein–Moss effect and in the P^+-region due to wide gap. The influence of surface recombination is also prevented by the use of suitable passivation. Passivation of HgCdTe has been done by several techniques which comprehensive review was given by Nemirovsky and

Bahir [26]. Recently, however, most laboratories have been using CdTe or CdZnTe (deposited by MBE, MOCVD, sputtering and e-beam evaporation) for photodiode passivation [27]. For example; the important element of the DLHJ structure are an In-doped ($N_d \approx 10^{15}$ cm^{-3}) HgCdTe absorber layer with a wider band-gap cap layer grown by LPE (MBE or MOCVD), arsenic diffusion (or implantation; $N_a \approx 10^{18}$ cm^{-3}), a passivation layer, metal contacts to the diode, and indium bumps for mating to the readout IC multiplexer.

It appears, that for the lowest doping levels, achievable in controllable manner in the base regions of photodiodes ($N_a = 5 \times 10^{15}$ cm^{-3} for n$^+$–p structure, and $N_d = 5 \times 10^{14}$ cm^{-3} for p$^+$–n structure), the performance of both types of photodiodes is comparable for a given cutoff wavelength and temperature [28].

The dependence of the base region diffusion limited R_oA product on the long wavelength cutoff for P-on-n LWIR HgCdTe photodiodes at different temperatures is shown in Fig. 10. This figure also includes the experimental data reported by many authors for DLHJ p-on-n structures. The upper experimental data are situated about a half of an order below ultimate theoretical predictions. With a lowering of the operation temperature of photodiodes, the discrepancy between the theoretical curves and experimental data increases, which is due to additional currents in the junctions (such as tunnelling current or surface leakage current) that are not considered. Photodiodes with lower performance usually contain metallurgical defects such as dislocation clusters and loops, pin holes, striations, Te inclusions, and heavy terracing. It should be noticed that the upper experimental data in very long wavelength range (above 14 μm) at lower temperature (40 K) coincides very well with theoretical predictions.

Fig. 11 presents a comprehensive comparison of the performance of MWIR P-on-n HgCdTe photodiodes on CdZnTe and Si substrates for cutoff wavelengths ranging from 3.5 to 5 μm. The devices with highest performance are processed from MBE-grown epilayers on bulk CdZnTe substrates. The shorter cutoff devices (with $\lambda_c \approx 3$ μm) are diffusion-limited down to at least 125 K. The devices with longer cutoff wavelength (with $\lambda_c \approx 5$

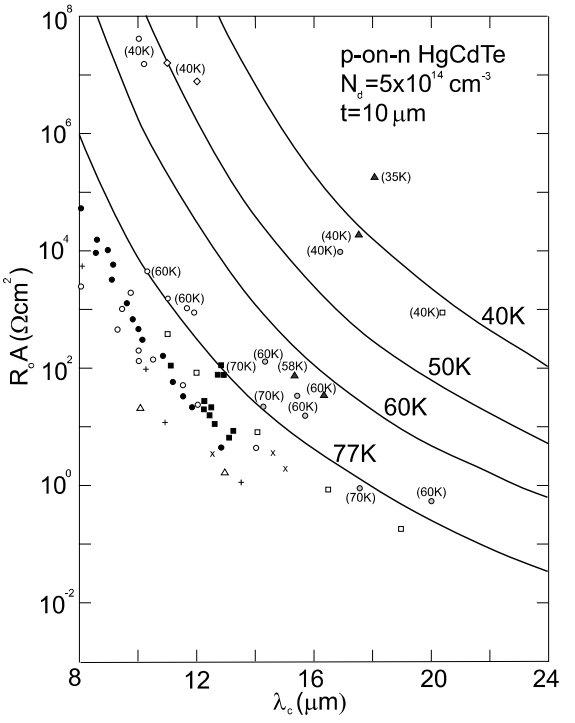

Fig. 10. Dependence of the R_oA product on the long wavelength cutoff for LWIR p$^+$–n HgCdTe photodiodes at temperatures $\leqslant 77$ K. The solid lines are calculated assuming that the performance of photodiodes are due to thermal generation governed by the Auger mechanism in the base n-type region of photodiodes with $t = 10$ μm and $N_d = 5 \times 10^{14}$ cm^{-3}. The experimental values are taken from different papers.

μm) appear to be diffusion-limited down to ≈110 K. Below this temperature the experimental data obscure the probable onset of generation-recombination and/or tunnelling current limitations.

Up to the present, photovoltaic HgCdTe FPAs have been mainly based on p-type material. Linear (240, 288, 480, and 960 elements), 2D scanning arrays with time delay and integration (TDI), and 2D staring formats from 32×32 up to 2048×2048 have been made [18]. Pixel sizes ranging from 18 μm square to over 1 mm have been demonstrated. The best results have been obtained using hybrid architecture.

4.4. Photoemissive PtSi Schottky-barrier detectors

The most popular Schottky-barrier detector is the PtSi detector which can be used for the

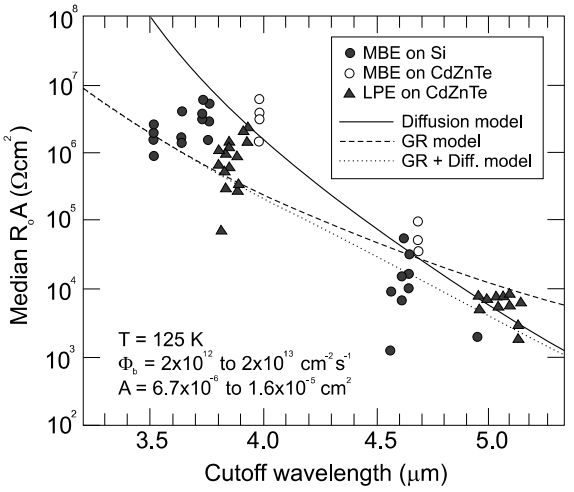

Fig. 11. Comparison of 125 K detector performance for MWIR HgCdTe photodiodes grown on Si and CdZnTe by MBE and photodiodes grown on CdZnTe by LPE. Each data point represents an array-median R_oA product measured at 125 K (after Ref. [29]).

detection in the 3–5 μm spectral range [30,31]. Radiation is transmitted through the p-type silicon and is absorbed in the metal PtSi (not in the semiconductor), producing hot holes which are then emitted over the potential barrier into the silicon, leaving the silicide charged negatively. Negative charge of silicide is transferred to a CCD by the direct charge injection method.

The effective quantum efficiency in the 3–5 μm atmospheric window is very low, of the order of 1%, but useful sensitivity is obtained by means of near full frame integration in area arrays. The quantum efficiency has been improved by thinning PtSi film and implementation of an "optical cavity". Due to very low quantum efficiency, the operating temperature of Schottky-barrier photoemissive detectors is lower than another types of IR photon detectors (see Fig. 5).

Schottky photoemission is independent of such factors as semiconductor doping, minority carrier lifetime, and alloy composition, and, as a result of this, has spatial uniformity characteristics that are far superior to those of other detector technologies. Uniformity is only limited by the geometric definition of the detectors.

Most of the reported Schottky-barrier FPAs have the interline transfer CCD architecture. Using a 1.2 μm charge sweep device technology, a large fill factor of 71% was achieved with a 26×20 μm^2 pixel in the 512×512 monolithic structure [31]. The noise equivalent temperature difference (NETD) was estimated as 0.033 K with $f/1.2$ optics at 300 K. The 1040×1040 element CSD FPA has the smallest pixel size (17×17 μm^2) among 2D IR FPAs. Current PtSi Schottky-barrier FPAs are mainly manufactured in 150 mm wafer process lines with around 1 μm lithography technologies; the most advanced Si technology offers 200 mm wafers process with 0.25 mm design rules. However, the performance of monolithic PtSi Schottky-barrier FPAs has reached a plateau, and a slow progress from now on is expected.

Various semiconductor photoemissive structures for far IR detection have been discussed by Perera [32].

4.5. Extrinsic photoconductors

Extrinsic photoresistors are used in a wide range of the IR spectrum extending from a few μm to ≈300 μm. They are the principal detectors operating in the range $\lambda > 20$ μm [33]. Detectors based on silicon and germanium have found the widest application as compared with extrinsic photodetectors on other materials. Si has several advantages over Ge; for example, three orders of magnitude higher impurity solubilities are attainable, hence thinner detectors with better spatial resolution can be fabricated from silicon. Si has lower dielectric constant than Ge, and the related device technology of Si has now been more thoroughly developed, including contacting methods, surface passivation and mature MOS and CCD technologies. Moreover, Si detectors are characterized by superior hardness in nuclear radiation environments. Fig. 12 illustrates the spectral response for several extrinsic detectors.

The availability of a highly developed silicon MOS technology facilities the integration of large detector arrays with charge-transfer devices for readout and signal processing. The well-established technology also helps in the manufacturing of uniform detector arrays and the formation of

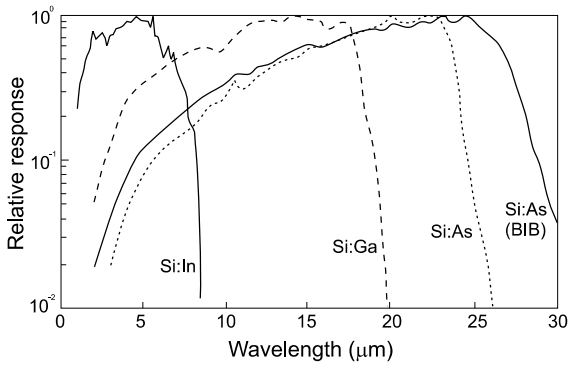

Fig. 12. Examples of extrinsic silicon detector spectral response. Shown are Si:In, Si:Ga, and Si:As bulk detectors and a Si:As BIB (after Ref. [34]).

low-noise contacts. Although the potential of large extrinsic silicon FPAs for terrestrial applications has been examined, interest has declined in favour of HgCdTe and InSb with their more convenient operating temperatures. Strong interest in doped silicon continues for space applications, particularly in low-background flux and for wavelengths from 13 to 20 μm, where compositional control is difficult for HgCdTe. The shallower impurity energies in germanium allow detectors with spectral response up to beyond 100 μm wavelength and major interest still exists in extrinsic germanium for wavelengths beyond about 20 μm.

To maximize the quantum efficiency and detectivity of extrinsic photoconductors, the doping level should be as high as possible. This idea is realized in blocked impurity band (BIB) devices. The longer spectral response of the BIB Si:As device compared with the bulk Si:As device (see Fig. 12) is due to the higher doping level in the former that reduces the binding energy of an electron. For a detailed analysis of the BIB detector see Szmulowicz and Madarsz [35].

BIB devices made from either doped silicon or doped germanium are sensitive in the IR wavelength range of 2 and 220 μm. BIB devices in large staring array formats are now becoming commercially available. The best results have been achieved to date for Si:As BIB hybrid FPAs produced by Hughes Technology Center in Carlsbad [36,37] and Rockwell International Science Center in Anaheim [38]. Hybrid FPAs with Si:As BIB detectors operating in 4–10 K temperature range have been optimised for low, moderate, and high IR backgrounds. The 256×256 format with 30 μm pixels and 240×320 format with 50 μm pixels are available for low- and high-background applications, respectively. Antimony-doped silicon (Si:Sb) arrays and 128×128 pixel Si:Sb hybrid FPAs having response to wavelengths >40 μm have been also demonstrated, primarily for use at low and moderate backgrounds. Germanium BIB devices have been developed on an experimental basis, but they have not been reported in large 2D array formats yet.

4.6. GaAs/AlGaAs QWIPs

Among the different types of quantum well IR photodetectors (QWIPs), technology of the GaAs/AlGaAs multiple quantum well detectors is the most mature [39,40].

QWIP technology is based on the well-developed A^3B^5 material system, which has a large industrial base with a number of military and commercial applications. QWIP cannot compete with HgCdTe photodiode as the single device especially at higher temperature operation (>70 K) due to fundamental limitations associated with intersubband transitions [17]. However, the advantage of HgCdTe is less distinct in temperature range below 50 K due to problems involved in a HgCdTe material (p-type doping, Shockley–Read recombination, trap-assisted tunnelling, surface and interface instabilities). Even though that QWIP is a photoconductor, several its properties such as high impedance, fast response time, long integration time, and low power consumption, well comply requirements of large FPAs fabrication. Due to the high material quality at low temperature, QWIP has potential advantages over HgCdTe for VLWIR FPA applications in terms of the array size, uniformity, yield and cost of the systems.

Fig. 13 shows two detector configurations used in fabrication of QWIP FPAs. In the bound-to-continuum QWIP the photoelectron can escape from the quantum well to the continuum transport states without being required to tunnel through the

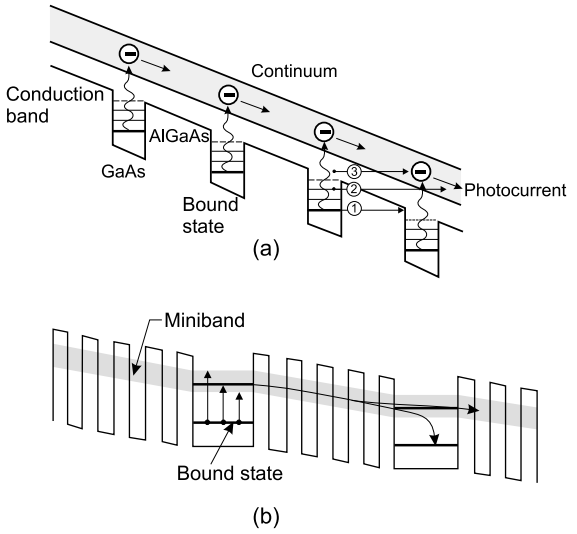

Fig. 13. Band diagram of demonstrated QWIP structures: (a) bound-to-extended and (b) bound-to-miniband. Three mechanisms creating dark current are also shown in (a): ground-state sequential tunnelling (1), intermediate thermally assisted tunnelling (2), and thermionic emission (3). The grey indicates extended states through which current flows.

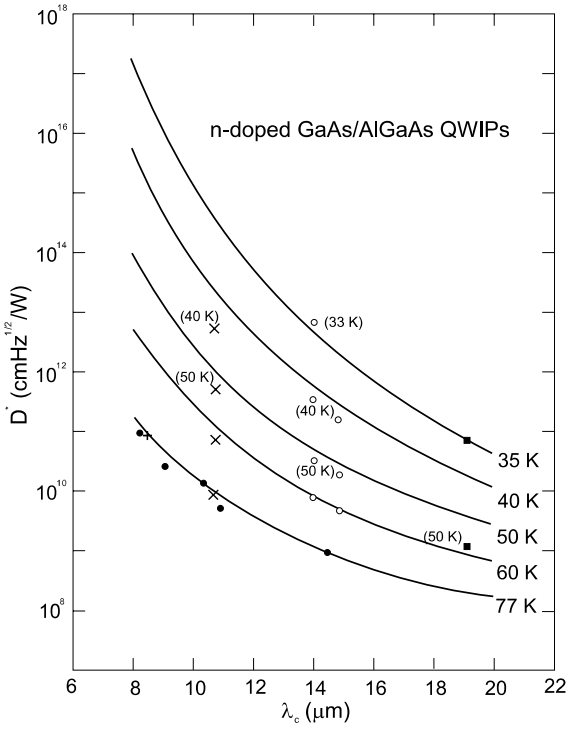

Fig. 14. Detectivity versus cutoff wavelength for n-doped GaAs/AlGaAs QWIPs at temperatures $\leqslant 77$ K. The solid lines are theoretically calculated. The experimental data are taken from different papers (after Ref. [41]).

barrier. As a result, the voltage bias required to efficiently collect the photoelectrons can be reduced dramatically, thereby lowering the dark current. It appears that the dark current decreases significantly when the first excited state is dropped from the continuum to the well top without sacrificing the responsivity.

In a miniband transport QWIP (see Fig. 13(b)), IR radiation is absorbed in the doped quantum wells, exciting an electron into the miniband and transporting it in the miniband until it is collected or recaptured into another quantum well. The miniband QWIPs show lower photoconductive gain than bound-to-continuum QWIPs because the photoexcited electron transport occurs in the miniband where electrons have to transport through many thin heterobarriers resulting in a lower mobility.

Rogalski [41] has used simple analytical expressions for detector parameters described by Andersson [42]. Fig. 14 shows the dependence of detectivity on the long wavelength cutoff for n-type GaAs/AlGaAs QWIPs at different temperatures. The satisfactory agreement with experimental data in wide range of cutoff wavelength $8 \leqslant \lambda_c \leqslant 19$ μm and temperature $35 \leqslant T \leqslant 77$ K has been obtained, considering the samples having different doping, different methods of crystal growth, different spectral widths, different excited states, and even in one case a different materials system (InGaAs).

A key factor in QWIP FPA performance is the light-coupling scheme. A distinct feature of QWIPs is that the optical absorption strength is proportional to an incident photon's electric-field polarisation component normal to the quantum wells. For imaging, it is necessary to be able to couple light uniformly to 2D arrays of these detectors, so a diffraction grating or other similar structure is typically fabricated on one side of the detectors to redirect a normally incident photon into propagation angles more favourable for absorption. The pixels of 2D arrays are thinned to about 5 μm in thickness. The thinning traps dif-

fracted light inside the illuminated pixels, increasing responsivity and eliminating crosstalk. The thinning also allows the detector array to stretch and accommodate the thermal expansion mismatch with the Si ROIC.

Gunapala and co-workers at Jet Propulsion Laboratory (JPL) demonstrated a 256×256 QWIP FPA in an Amber hand-held camera. The current state of the art for QWIP FPA size has been 640×480 recently demonstrated by JPL [43,44] and Lockheed Martin [45]. The measured mean NEDT of the QWIP camera was 36 mK at an operating temperature of $T = 70$ K at 300 K background [44].

4.7. Thermal detectors

IR semiconductor imagers use cryogenic or thermoelectric coolers, complex IR optics, and expensive sensor materials. Typical costs of cryogenically cooled imagers of around $50 000 restrict their installation to critical military applications allowing conducting of operations in complete darkness. Very encouraging results have been obtained with micromachined silicon bolometer arrays and pyroelectric detector arrays. Several countries have demonstrated imagers with NEDT of 100 mK or better, and the cost of simple systems is sometimes below $10 000. It is expected that high-performance imager system costs will be reduced to less than $1000 [46] and above IR cameras will become widely available in the near future. Although developed for military applications, low-cost IR imagers are used in non-military applications such as: drivers aid, aircraft aid, industrial process monitoring, community services, firefighting, portable mine detection, night vision, border surveillance, law enforcement, search and rescue, etc.

4.7.1. Micromachined silicon bolometers

The most popular thermistor material used in fabrication of the micromachined silicon bolometers is vanadium dioxide, VO_2. From the point of view of IR imaging application, probably the most important property of VO_2 is its high negative temperature coefficient of resistance (TCR) at ambient temperature, which exceeds 4% per degree for single element bolometer and about 2% for FPA.

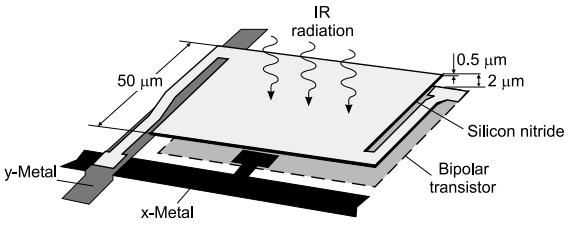

Fig. 15. Bridge structure of Honeywell microbolometer (after Ref. [47]).

The final microbolometer pixel structure is shown in Fig. 15. The microbolometer consists of a 0.5 μm thick bridge of Si_3N_4 suspended about 2 μm above the underlying silicon substrate. The use of a vacuum gap of ≈2.5 μm, together with a quarter wave resonant cavity between the bolometer and the underlying substrate, can produce a reflector for wavelengths near 10 μm. The bridge is supported by two narrow legs of Si_3N_4. The Si_3N_4 legs provide the thermal isolation between the microbolometer and the heat-sink readout substrate and support conductive films for electrical connection. A bipolar input amplifier is normally required, and this can be obtained with biCMOS processing technology. Encapsulated in the centre of the Si_3N_4 bridge is a thin layer (500 Å) of polycrystalline VO_x.

Honeywell has licensed this technology to several companies for the development and production of uncooled FPAs for commercial and military systems. At present, the compact 320×240 microbolometer cameras are produced by Raytheon, Boeing, and Lockheed Martin in the United States. The US government allowed these manufactures to sell their devices to foreign countries, but not to divulge manufacturing technologies. In recent years, several countries, including the United Kingdom, Japan, Korea, and France have picked up the ball, determined to develop their own uncooled imaging systems. As a result, although the US has a significant lead, some of the most exciting and promising developments for low-cost uncooled IR systems may come from non-US companies, e.g., microbolometr FPAs with series p–n junction elaborated by Mitsubishi

Electric [48]. This approach is unique, based on an all-silicon version of microbolometer.

The 240×320 arrays of 50 μm microbolometers are fabricated on industry-standard wafer (4 in. diameter) complete with monolithic readout circuits integrated into underlying silicon. Radford et al. [49] have reported a 240×320 pixel array with 50 μm square vanadium oxide pixels, for which the average NETD ($f/1$ optics) was 8.6 mK. Larger arrays size was described by Altman and colleagues at Lockheed Martin [50]; they reported a 640×480 FPA with 28×28 m^2 pixels with NETD ($f/1$ optics) of about 60 mK.

At present, several research programmes are focused towards enhancement of performance level in excess of 10^9 cm Hz$^{1/2}$ W^{-1}. It is anticipated that new materials will form the basis of the next generation of semiconductor film bolometers. The most promising material appears to be amorphous silicon [51].

4.7.2. Pyroelectric detectors

The imaging systems based on pyroelectric arrays, usually need to be operated with optical modulators which chop or defocus the incoming radiation. This may be an important limitation for many applications in which chopperless operation is highly desirable (e.g., guided munitions). Hitherto, most of the ferroelectric detectors have been operated well-below Curie temperature T_C, where the polarisation is not affected by changes in ambient temperature. It is, however, possible to operate ferroelectrics at or above T_C, with an applied bias field, in the mode of a ''dielectric bolometer''.

Several materials have been examined in dielectric bolometer mode. Barium strontium titanate (BST) ceramic is a relatively well-behaved material with a very high permittivity. Texas instruments (TI) has improved the performance of pyroelectric FPAs using a bias voltage applied to maintain and optimise the pyroelectric effect near the phase transition [52]. Fig. 16 shows details of the completed pyroelectric detector device structure. For the United Kingdom array programme lead scandium tantalate (PST) material has been chosen [53].

Although many applications for this hybrid array technology have been identified, and imagers employing these arrays are in mass production, no hybrid technology advances are foreseen. The reason is that the thermal conductance of the bump bonds is so high that the array NETD ($f/1$ optics) is limited to about 50 mK. Pyroelectric array technology therefore is moving toward monolithic silicon microstructure technology. The monolithic process should have fewer steps and shorter cycle time. Most ferroelectrics tend to lose their interesting properties as the thickness is reduced. However, some ferroelectric materials seem to maintain their properties better than others. This seems particularly true for lead titanate ($PbTiO_3$) and related materials, whereas BST, the material used in hybrid detectors, does not hold its properties well in thin-film form. Various techniques for the deposition of thin ferroelectric films have been investigated, including radio frequency magnetron sputtering, dual ion beam sputtering, sol–gel processing, and laser ablation.

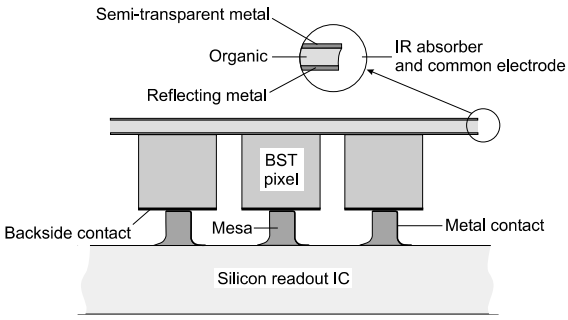

Fig. 16. BST dielectric bolometer pixel (after Ref. [31]).

5. Dual-band IR focal plane arrays

Multicolour capabilities are highly desirable for advance IR systems. Systems that gather data in separate IR spectral bands can discriminate both absolute temperature and unique signatures of objects in the scene. By providing this new dimension of contrast, multiband detection also enables advanced colour processing algorithms to further improve sensitivity above that of single-colour devices. Currently, multispectral systems rely on cumbersome imaging techniques that either disperse the optical signal across multiple IR FPAs

or use a filter wheel to spectrally discriminate the image focused on single FPA. Consequently, these approaches are expensive in terms of size, complexity, and cooling requirements. Both HgCdTe photodiodes and QWIPs offer the multicolour capability in the MWIR and LWIR range.

Considerable progress has been recently demonstrated in multispectral HgCdTe detectors employing MBE and MOCVD for the growth of variety devices [54–61]. Also QWIP's technology demonstrates considerably progress in fabrication of multicolour FPAs [40,44,62–66]. Devices for the sequential and simultaneous detection of two closely spaced sub-bands in the MWIR and LWIR radiation have been demonstrated.

5.1. Dual-band HgCdTe FPAs

The two-colour detector arrays are usually based upon an n–P–N HgCdTe triple layer heterojunction (TLHJ) design. The TLHJ detectors consist of back-to-back photovoltaic p–n junctions. This device architecture is realised by placing a longer wavelength HgCdTe photodiode simply behind shorter wavelength photodiode. Also quaternary device structure is used [60].

Both sequential-mode and simultaneous mode detectors are fabricated from the multilayer materials. The mode of detection is determined by the fabrication process. Figs. 17 and 18 show the elements of arrays of two-colour photovoltaic unit cells in both modes. The sequential-mode detector has a single indium bump per unit cell that permits sequential bias selectivity of the spectral bands associated with operating tandem photodiodes. The problems with the bias-selectable device are the following: its construction does not allow independent selection of the optimum bias voltage for each photodiode, and there can be substantial medium wavelength crosstalk in the long wavelength detector. To overcome the problems of the bias-selectable device, the independently accessed

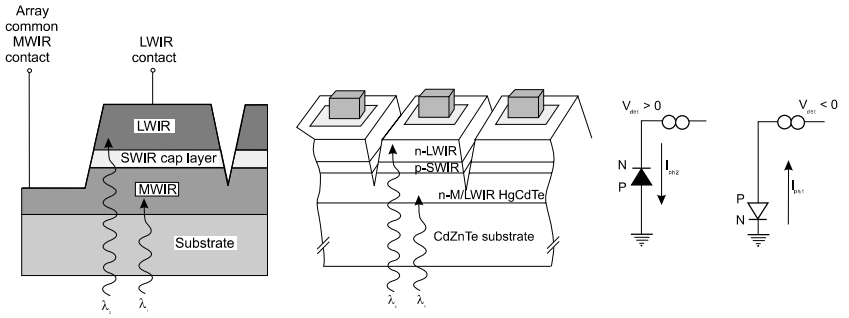

Fig. 17. Cross-section of integrated two-colour detectors in an n–P–N layer structure for sequential operating mode.

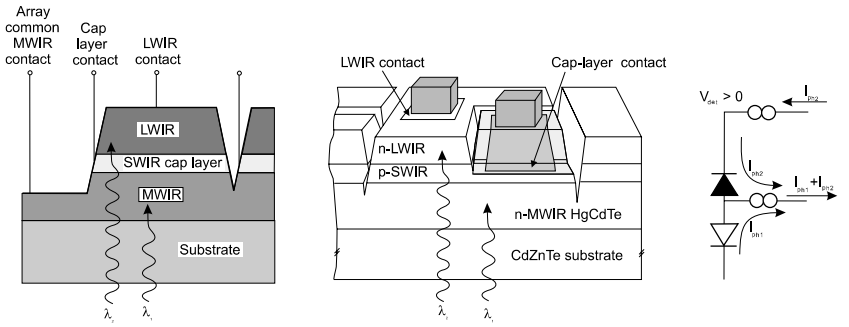

Fig. 18. Cross-section of integrated two-colour detectors in an n–P–N layer structure for simultaneous operating mode.

back-to-back photodiode dual-band detectors have been proposed. The simultaneous mode detector employs an additional electrical contact to the shared-type centre layer so that each junction can be accessed independently with both signal channels integrated simultaneously. Longwave band fill factor is reduced from that of the midwave, since some junction area is sacrificed to provide contact to the buried cap layer, and spatial coincidence is altered.

Critical step in device formation is connected with in situ doped p-type As-doped layer with good structural and electrical properties to prevent internal gain from generating spectral crosstalk. The band-gap engineering effort consists of increasing the CdTe mole fraction and the effective thickness of the p-type layer to suppress out-off-band carriers from being collected at the terminal.

Fig. 19 shows examples of spectral response from MWIR/MWIR, MWIR/LWIR, and LWIR/LWIR two-colour devices.

Fill factors of 128×128 MWIR/MWIR FPAs as high as 80% were achieved by using a single mesa structure to accommodate the two indium bump contacts required for each unit cell with 50 μm size [9]. The NEDT for both bands was below 25 mK and imagery was acquired at temperatures as high as 180 K with no visible degradation in image quality. The camera used for these measurements had a 50 mm, $f/2.3$ lens.

Recently, Rockwell and Boeing have extended a single-colour DLHJ planar technology to two-colour architecture [61]. A cross-section of a typical backside illuminated pixel is shown in Fig. 20. The band 1 absorber (shorter wavelength) is grown first, with the band 2 absorber (longer wavelength)

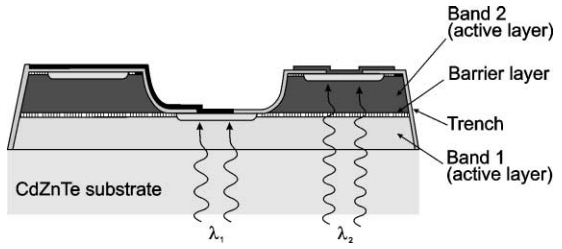

Fig. 20. Two-colour simultaneous unipolar architecture (after Ref. [61]).

grown on top. To prevent diffusion of carriers between two bands, a wide-band-gap 1 μm thick layer separates these absorbing layers. The diodes are formed by implanting arsenic as a p-type dopant and activating with an anneal giving unipolar operation for both bands. The band 2 implanted area is a concentric ring around the band 1 dimple. Because the lateral carrier diffusion length is larger than the pixel pitch in the MWIR material and the band 1 junction is small, the pixel is isolated by dry etching a trench around each pixel to reduce carrier crosstalk. The entire structure is capped with a slightly wider band-gap layer to reduce surface recombination and simplify passivation. Two-colour 128×128 FPAs with low-10^{13} $cm^{-2}\,s^{-1}$ background limited detectivity performance have been obtained for MWIR (3–5 μm) devices at $T < 130$ K and for LWIR (8–10 μm) devices at $T \approx 80$ K.

5.2. Dual-band QWIP FPAs

Device capable of simultaneously detecting two separate wavelengths can be fabricated by vertical stacking of the different QWIP layers during epitaxial growth (see Fig. 21). Separate bias voltages

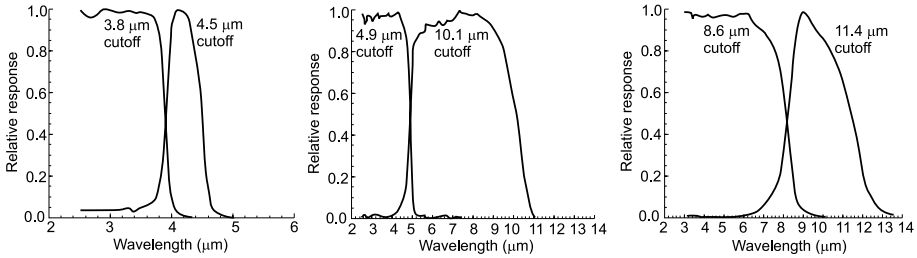

Fig. 19. Spectral response curves for two-colour HgCdTe detectors in various dual-band combinations of spectral bands (after Ref. [9]).

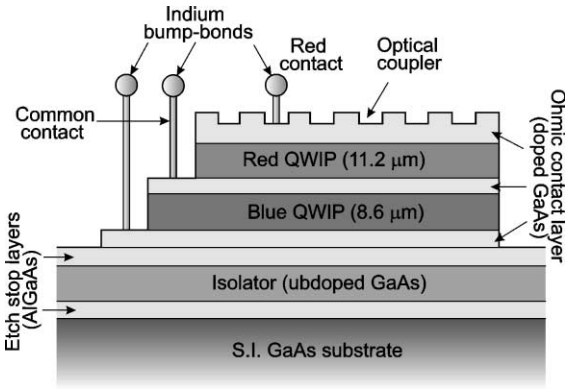

Fig. 21. Structure of two-colour stacked QWIP (after Ref. [63]).

can be applied to each QWIP simultaneously via the doped contact layers that separate the multiple quantum well detector heterostructures.

Typical operating temperature for QWIP detectors is in the region of 40–100 K. The bias across each QWIP can be adjusted separately, although it is desirable to apply the same bias to both colours. As shown in Fig. 22, the responsivity of both QWIPs is around 300–350 mA/W at a temperature 40 K and at an operating bias of +1.5 μm applied to common contact. It appears that the complex two-colour processing has not compromised the electrical and optical quality of either colour in the two-colour device.

A key factor in QWIP FPA performance is the light-coupling scheme. Different light-coupling mechanisms are used in QWIPs. Most QWIP arrays use 2D grating, which is very wavelength dependent, and efficiency gets lower when the pixel size gets smaller. Lockheed Martin has used rectangular and rotated rectangular 2D gratings for their two-colour LW/LW FPAs. Although random reflectors have achieved relatively high quantum efficiencies with large test device structure, it is not possible to achieve the similar high quantum efficiencies with random reflectors on small FPA pixels due to the reduced width-to-height aspect rations. In addition, it is difficult to fabricate random reflectors for shorter wavelength detectors relative to long wavelength detectors due to the fact that feature sizes of random reflectors are linearly proportional to the peak wavelength of the detectors. As a result, the quantum efficiency becomes a more difficult issue for QWIP multicolour FPA than for single colour.

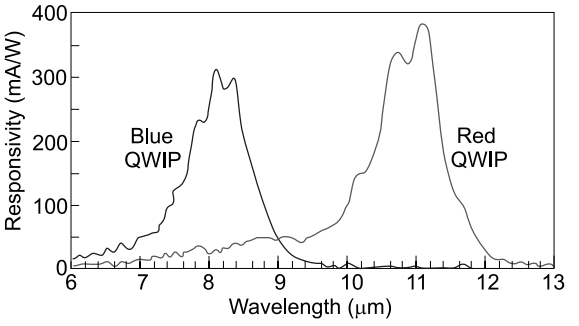

Fig. 22. Typical responsivity spectra at 40 K and a common bias of 1.5 V, recorded simultaneously for two QWIPs in the same pixel (after Ref. [63]).

Two-colour detectors that cover both MWIR and LWIR atmospheric windows are especially important in many applications. To cover MWIR range a strained layer InGaAs/AlGaAs material system is used. InGaAs in MWIR stack produces high in-plane compressive stain which enhances the responsivity [67]. The MWIR/LWIR FPAs fabricated by Sanders consist of an 8.6 μm GaAs/AlGaAs QWIP on top of 4.7 μm strained InGaAs/GaAs/AlGaAs heterostructure. The fabrication process allowed fill factors of 85% and 80% for the MW and LW detectors. The first FPAs with this configuration had an operability in excess of 97%, and NETD value better 35 mK.

Recently, Gunapala et al. [64] have demonstrated the first 8–9 and 14–15 μm two-colour imaging camera based on a 640 × 486 dual-band QWIP FPA, which can be processed with dual or triple contacts to access the CMOS readout multiplexer. Single indium bump per pixel is usable only in the case of interlace readout scheme (i.e., odd rows for one colour and the even rows for the other colour) which uses an existing single-colour CMOS readout multiplexer. However, the disadvantage is that it does not provide a full fill factor for both wavelength bands.

The device structure, shown in Fig. 23, consists of a 30 period stack (500 Å AlGaAs barrier and a 60 Å GaAs well) of very LWIR (VLWIR) structure and a second 18 period stack (500 Å AlGaAs

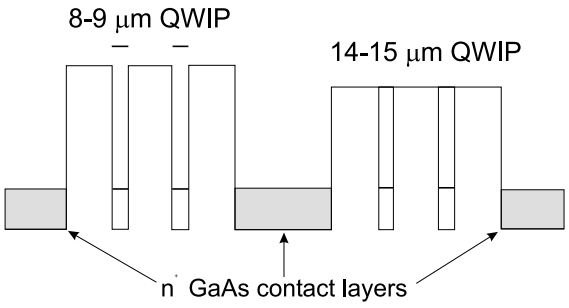

Fig. 23. Conduction band diagram of the LWIR and VLWIR two-colour detector (after Ref. [64]).

barrier and a 40 Å GaAs well) of LWIR structure separated by a heavily doped 0.5 μm thick intermediate GaAs contact layer. The VLWIR QWIP structure has been designed to have a bound-to-quasibound intersubband absorption peak at 14.5 μm, whereas the LWIR QWIP structure has been designed to have a bound-to-continuum intersubband absorption peak at 8.5 μm, since photocurrent and dark current of the LWIR device structure is relatively small compared to the VLWIR portion of the device structure.

Fig. 24 shows schematic side view of the interlace dual-band GaAs/AlGaAs FPA. Two different 2D periodic grating structures were designed to independently couple the 8–9 and 14–15 μm radiation into detector pixels in even and odd rows of the FPAs. The top 0.7 μm thick GaAs cap layer was used to fabricate the light-coupling 2D periodic gratings for 8–9 μm detector pixels, whereas the light-coupling 2D periodic gratings of the 14–15 μm detector pixels were fabricated through LWIR MQW layers. In such a way, this grating scheme short circuited all 8–9 μm sensitive detectors in all odd rows of the FPAs. The FPA was back-illuminated through the flat thinned substrate membrane (≈1000 Å). Very thin substrate adapts the thermal expansion and contraction coefficient of the silicon readout multiplexer, completely eliminates the thermal mismatch problem between the silicon readout and the GaAs based detector array, completely eliminates pixel-to-pixel crosstalk, and finally, significantly enhances an optical coupling of IR radiation into QWIP pixels.

The performance of dual-band FPAs were tested at a background temperature of 300 K, with $f/2$ cold stop, and at 30 Hz frame rate. The mean value of quantum efficiency at operating temperature $T = 40$ K and bias $V_B = -2$ V is 12.9% and 8.9% in LW and VLW spectral range, respectively. The estimated NEDT of LWIR and VLWIR detectors at 40 K are 36 and 44 mK, respectively.

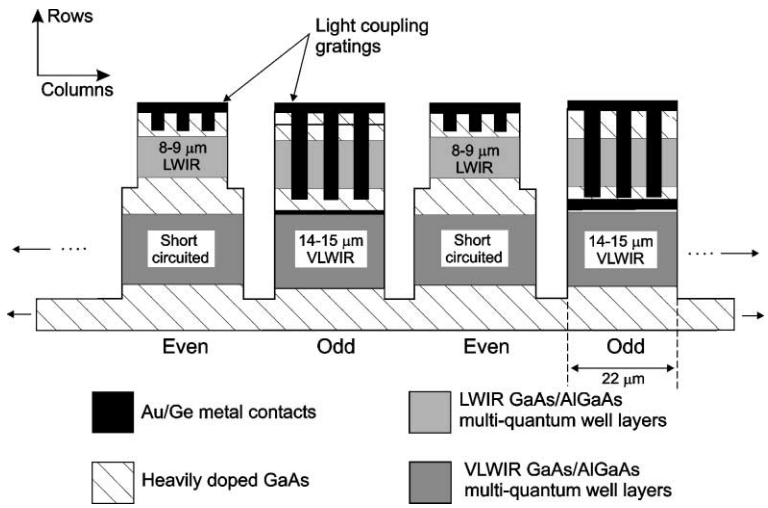

Fig. 24. Structure cross-section of the interlace dual-band FPA (after Ref. [64]).

6. Anticipated evolution of IR technology in the near future

The future applications of IR detector systems require:

- higher pixel sensitivity,
- further increase in pixel density to above 10^6 pixels,
- cost reduction in IR imaging array systems through the use of less cooling sensor technology combined with integration of detectors and signal-processing functions (with much more on-chip signal processing),
- improvement in the functionality of IR imaging arrays through development of multispectral sensors.

To reduce the real cost of the IR image systems, one must take action on all the elements, which make up the cost to the user. The cost can be broken down into three parts: the chip (detector + ROIC), the dewar, integration and tests. The user must add the cryogenic machine cost that is not negligible compared to the component one's. This explains why the cost of PtSi or QWIPs is not markedly less than that of photon detectors of the same complexity, even though the raw materials (silicon and GaAs) is much less than for HgCdTe. A possible reduction in the purchase price is counterbalanced by a significant increase in operating costs.

Detector maturity is a function of the accumulated experience and development effort, the complexity of the device required, and the inherent difficulty presented by the material technology. At present, HgCdTe photodiodes and BIB extrinsic silicon detectors are not fully mature. PtSi technology is mature and has received a plateau. Other two detector technologies such as InSb and silicon bolometers are still evolving significantly as applications for larger array configurations and smaller pixel sizes continue to push the technology.

Thermal detector arrays will increase in size and improve in thermal sensitivity to a level satisfying high performance applications at ambient temperature. It is supposed that the silicon microbolometers arrays and the monolithic pyroelectric arrays will capture the low-cost markets. Current uncooled bolometer FPAs have achieved NEDT less than 10 mK with $f/1$ optics, what open the door to the use of less expensive slower optical systems.

It is supposed that sales of IR thermal imaging equipment to the automobile market will begin to rapidly change the relative ratio between military/government and commercial IR markets. Today only about 10% of the market is commercial. After a decade the commercial market can grow to over 70% in volume and 40% in value, largely connected with volume production of uncooled imagers for automobile driving [9]. In large volume production for automobiles drivers the cost of uncooled imaging systems will decrease to below $1000. Of course, these systems will cover other segments of the transportation industry: trucks, trains, ships, barges, buses, and airplanes.

For same applications requiring uncooled detectors, the slow response speed is unacceptable. Recently, a number of concepts (e.g., non-equilibrium device [68], multijunction HgCdTe photodiodes [69], optical immersion) and new materials (InAsSb, InAs/GaSb-based type II superlattices) [11] have been proposed to improve performance of photon detectors operating at near room temperature. The measurements show the possibility to achieve detectivity of $\approx 1 \times 10^9$ cm $Hz^{1/2}$ W^{-1} at the 8–9 μm range and potentially, the devices can be assembled in large FPAs.

Despite serious competition from alternative technologies and slower progress than expected, HgCdTe is unlikely to be seriously challenged for high-performance applications, applications requiring multispectral capability and fast response. The recent successes of competing cryogenically cooled detectors are due to technological, not fundamental issues. The steady progress in epitaxial technology would make HgCdTe devices much more affordable in the near future. The much higher operation temperature of HgCdTe, compared to Schottky-barrier devices and low-dimensional solid devices, may become a decisive argument in this case.

The fundamental performance limits of HgCdTe photodiodes have not been reached yet. Continued development of the in situ vapour

phase epitaxy methods (MBE and MOCVD) will allow band-gap engineering heterojunction devices of increasing quality and complexity. Also continued development of epitaxial growth on alternative substrates such as silicon will reduce the cost of 2D arrays. Development of dual-band array will continue and three-band detectors will soon be demonstrated. To provide high resolution spectroscopic imaging larger HgCdTe FPAs will be used in Fourier-transform (FT) interferometers. Photodiodes will replace photoresistors for detection out to 15 μm since they characterised by more linear response.

The situation concerning quantum well structures and superlattices is not clear; however, unique detection capabilities may arise from the low-dimensional solids. Situation of LWIR QWIPs is clear. The initial results show promise for the growth of QWIPs on silicon wafers and applications for integration with silicon-based electronics. It is expected that the QWIP hand-held, cost-effective camera will find imaging and spectroscopy applications in LWIR spectral band. Powerful possibilities of QWIP technology are connected with VLWIR FPA applications and with multicolour detection. Three-band and four-band FPAs will soon be demonstrated in near the future.

A new IR detector concept is microelectromechanical structures (MEMSs). This technology is a marriage of photolithography and mechanics. FPAs based on MEMS technology and a visible optical readout system may offer lower-cost LWIR imaging systems [70].

Finally, considerable development of signal-processing function into FPAs can be anticipated.

References

[1] W. Herschel, Experiments on the refrangibility of the invisible rays of the Sun, Philos. Trans. Roy. Soc. London 90 (1800) 284.
[2] R.A. Smith, F.E. Jones, R.P. Chasmar, The Detection and Measurement of Infrared Radiation, Clarendon, Oxford, 1958.
[3] P.W. Kruse, L.D. McGlauchlin, R.B. McQuistan, Elements of Infrared Technology, Wiley, New York, 1962.
[4] E.S. Barr, Historical survey of the early development of the infrared spectral region, Am. J. Phys. 28 (1960) 42–54.
[5] E.S. Barr, The infrared pioneers—II. Macedonio Melloni, Infrared Phys. 2 (1962) 67–73.
[6] E.S. Barr, The infrared pioneers—III. Samuel Pierpont Langley, Infrared Phys. 3 (1963) 195–206.
[7] T.W. Case, Notes on the change of resistance of certain substrates in light, Phys. Rev. 9 (1917) 305–310.
[8] R.J. Cushman, Film-type infrared photoconductors, Proc. IRE 47 (1959) 1471–1475.
[9] P.R. Norton, Infrared detectors in the next millennium, Proc. SPIE 3698 (1999) 652–665.
[10] A. Rogalski, Infrared Detectors, Gordon and Breach Science Publishers, Amsterdam, 2000.
[11] M. Razeghi, Current status and future trends of infrared detectors, Opto-Electron. Rev. 6 (1998) 155–194.
[12] R.A. Wood, Uncooled microbolometer infrared sensor arrays, in: P. Capper, C.T. Elliott (Eds.), Infrared Detectors and Emitters: Materials and Devices, Kluwer Academic Publishers, Boston, 2000, pp. 149–174.
[13] R.W. Whatmore, R. Watton, Pyroelectric materials and devices, in: P. Capper, C.T. Elliott (Eds.), Infrared Detectors and Emitters: Materials and Devices, Kluwer Academic Publishers, Boston, 2000, pp. 99–147.
[14] D.A. Scribner, M.R. Kruer, J.M. Killiany, Infrared focal plane array technology, Proc. IEEE 79 (1991) 66–85.
[15] P.R. Norton, Status of infrared detectors, Proc. SPIE 3379 (1998) 102–114.
[16] J. Piotrowski, W. Gawron, Ultimate performance of infrared photodetectors and figure of merit of detector material, Infrared Phys. Technol. 38 (1997) 63–68.
[17] A. Rogalski, Assessment of HgCdTe photodiodes and quantum well infrared photoconductors for long wavelength focal plane arrays, Infrared Phys. Technol. 40 (1999) 279–294.
[18] A. Rogalski, K. Adamiec, J. Rutkowski, Narrow-Gap Semiconductor Photodiodes, SPIE Press, Bellingham, 2000.
[19] L.J. Kozlowski, K. Vural, J.M. Arias, W.E. Tennant, R.E. DeWames, Performance of HgCdTe, InGaAs and quantum well GaAs/AlGaAs staring infrared focal plane arrays, Proc. SPIE 3182 (1997) 2–13.
[20] W.F.M. Micklethwaite, A.J. Johnson, InSb: materials and devices, in: P. Capper, C.T. Elliott (Eds.), Infrared Detectors and Emitters: Materials and Devices, Kluwer Academic Publishers, Boston, 2000, pp. 177–204.
[21] J.T. Wimmers, D.S. Smith, Characteristics of InSb photovoltaic detectors at 77 K and below, Proc. SPIE 364 (1983) 123–131.
[22] J.T. Wimmers, R.M. Davis, C.A. Niblack, D.S. Smith, Indium antimonide detector technology at Cincinnati Electronics Corporation, Proc. SPIE 930 (1988) 125–138.
[23] A.M. Fowler, I. Gatley, P. McIntyre, F.J. Vrba, A. Hoffman, ALADDIN, the 1024 × 1024 InSb array: design, description, and results,, Proc. SPIE 2816 (1996) 150–160.
[24] J.B. Varesi, R.E. Bornfreund, A.C. Childs, W.A. Radford, K.D. Maranowski, J.M. Peterson, S.M. Johnson, L.M. Giegerich, T.J. de Lyon, J.E. Jensen, Fabrication of high-performance large-format MWIR focal plane arrays from

MBE-grown HgCdTe on 4'' silicon substrates, J. Electron. Mater. 30 (2001) 566–573.
[25] M.B. Reine, Photovoltaic detectors in MCT, in: P. Capper, C.T. Elliott (Eds.), Infrared Detectors and Emitters: Materials and Devices, Kluwer Academic Publishers, Boston, 2000, pp. 279–312.
[26] Y. Nemirovsky, G. Bahir, Passivation of mercury cadmium telluride surfaces, J. Vac. Sci. Technol. A 7 (1989) 450–459.
[27] W.E. Tennant, C.A. Cockrum, J.B. Gilpin, M.A. Kinch, M.B. Reine, R.P. Ruth, Key issues in HgCdTe-based focal plane arrays: a industry perspective, J. Vac. Sci. Technol. B 10 (1992) 1359–1369.
[28] A. Rogalski, R. Ciupa, Long wavelength HgCdTe photodiodes: n^+-on-p versus p-on-n structures, J. Appl. Phys. 77 (1995) 3505–3512.
[29] T.J. de Lyon, R.D. Rajavel, J.A. Vigil, J.E. Jensen, O.K. Wu, C.A. Cockrum, S.M. Johnson, G.M. Venzor, S.L. Bailey, I. Kasai, W.L. Ahlgren, M.S. Smith, Molecular-beam epitaxial growth of HgCdTe infrared focal-plane arrays on silicon substrates for midwave infrared applications, J. Electron. Mater. 27 (1998) 550–555.
[30] M. Kimata, N. Tsubouchi, Schottky barrier photoemissive detectors, in: A. Rogalski (Ed.), Infrared Photon Detectors, SPIE Optical Engineering Press, Bellingham, 1995, pp. 299–349.
[31] M. Kimata, Metal silicide Schottky infrared detector arrays, in: P. Capper, C.T. Elliott (Eds.), Infrared Detectors and Emitters: Materials and Devices, Kluwer Academic Publishers, Boston, 2000, pp. 77–98.
[32] A.G.H. Perera, Semiconductor photoemissive structures for far infrared detection, in: M.H. Francombe (Ed.), Handbook of Thin Devices, vol. 2, Academic Press, San Diego, 2000, pp. 135–170.
[33] N. Sclar, Properties of doped silicon and germanium infrared detectors, Prog. Quant. Electr. 9 (1984) 149–257.
[34] P.R. Norton, Infrared image sensors, Opt. Eng. 30 (1991) 1649–1663.
[35] F. Szmulowicz, F.L. Madarsz, Blocked impurity band detectors—An analytical model: Figures of merit, J. Appl. Phys. 62 (1987) 2533–2540.
[36] J. Venzon, N. Lum, S. Freeman, G. Domingo, High-background, longwave IR focal plane array development using Si:As IBC detectors, Proc. SPIE 2475 (1995) 34–40.
[37] S. Solomon, A. Tribble, N. Lum, J. Venzon, G. Domingo, A. Hofman, M. Smith, High-background, longwave Si:As IBC 320×240 IR focal plane array, Proc. SPIE 2816 (1996) 161–168.
[38] M.G. Stapelbroeck, D.H. Seib, J.E. Huffman, R.A. Florence, Large-format blocked-impurity-band focal plane arrays for long wavelength infrared astronomy, Proc. SPIE 2476 (1995) 41–48.
[39] B.F. Levine, Quantum-well infrared photodetectors, J. Appl. Phys. 74 (1993) R1–R81.
[40] S.D. Gunapala, S.V. Bandara, Quantum well infrared photodetectors, in: M.H. Francombe (Ed.), Handbook of Thin Devices, vol. 2, Academic Press, San Diego, 2000, pp. 63–99.
[41] A. Rogalski, Quantum well infrared photodetectors among the other types of semiconductor infrared detectors, Infrared Phys. Technol. 38 (1997) 295–310.
[42] J.Y. Andersson, Dark current mechanisms and conditions of background radiation limitation of n-doped AlGaAs/GaAs quantum-well infrared detectors, J. Appl. Phys. 78 (1995) 6298–6304.
[43] S. Gunapala, S. Bandara, J. Liu, M. Sundaram, Sharp infrared eyes: the journey of QWIPs from concept to large inexpesive sensitive arrays in hand-held infrared cameras, Opto-Electron. Rev. 7 (1999) 271–282.
[44] S.D. Gunapala, S.V. Bandara, J.K. Liu, E.M. Luong, S.B. Rafol, J.M. Mumolo, D.Z. Ting, J.J. Bock, M.E. Ressler, M.W. Werner, P.D. LeVan, R. Chehayeb, C.A. Kukkonen, M. Levy, N. LeVan, M.A. Fauci, Recent developments and applications of quantum well infrared photodetector focal plane arrays, Opto-Electron. Rev. 9 (2001) 150–163.
[45] M. Sundaram, S.C. Wang, 2-color QWIP FPAs, Proc. SPIE 4028 (2000) 311–317.
[46] R.A. Wood, N.A. Foss, Micromachined bolometer arrays achieve low-cost imaging, Laser Focus World June (1993) 101–106.
[47] R.A. Wood, C.J. Han, P.W. Kruse, Integrated uncooled IR detector imaging arrays, Proc. IEEE Solid State Sensor and Actuator Workshop, Hilton Head Island, S.C., June, 1992, pp. 132–135.
[48] T. Ishikawa, M. Ueno, K. Endo, Y. Nakaki, H. Hata, T. Sone, M. Kimata, Low-cost 320×240 uncooled IRFPA using conventional silicon IC process, Opto-Electron. Rev. 7 (1999) 297–303.
[49] W. Radford, D. Murphy, A. Finch, K. Hay, A. Kennedy, M. Ray, A. Sayed, J. Wyles, R. Wyles, J. Varesi, E. Moody, F. Cheung, Sensitivity improvements in uncooled microbolometer FPAs, Proc. SPIE 3698 (1999) 119–130.
[50] M. Altman, B. Backer, M. Kohin, R. Blackwell, N. Butler, J. Cullen, Lockheed Martin 640×480 uncooled microbolometer camera, Proc. SPIE 3698 (1999) 137–143.
[51] C. Vedel, J.L. Martin, J.L. Ouvrier Buffet, J.L. Tissot, M. Vilan, J.J. Yon, Amorphous silicon based uncooled microbolometer IRFPA, Proc. SPIE 3698 (1999) 276–283.
[52] C.M. Hanson, Uncooled thermal imaging at Texas Instruments, Proc. SPIE 2020 (1993) 330–339.
[53] R.K. McEwen, P.A. Manning, European uncooled thermal imaging sensors, Proc. SPIE 3698 (1999) 322–337.
[54] R.D. Rajavel, D.M. Jamba, O.K. Wu, J.E. Jensen, J.A. Wilson, E.A. Patten, K. Kosai, P. Goetz, G.R. Chapman, W.A. Radford, High performance HgCdTe two-color infrared detectors grown by molecular beam epitaxy, J. Crystal Growth 175 (1997) 653–658.
[55] P. Mitra, S.L. Barnes, F.C. Case, M.B. Reine, P. O'Dette, R. Starr, A. Hairston, K. Kuhler, M.H. Weiler, B.L. Musicant, MOCVD of bandgap-engineered HgCdTe p–n–N–P dual-band infrared detector arrays, J. Electron. Mater. 26 (1997) 482–487.
[56] R.D. Rajavel, D.M. Jamba, J.E. Jensen, O.K. Wu, P.D. Brewer, J.A. Wilson, J.L. Johnson, E.A. Patten, K. Kasai,

J.T. Caulfield, P.M. Goetz, Molecular beam epitaxial growth and performance of integrated multispectral HgCdTe photodiodes for the detection of mid-wave infrared radiation, J. Crystal Growth 184 (1998) 1272–1278.

[57] R.D. Rajavel, D.M. Jamba, J.E. Jensen, O.K. Wu, J.A. Wilson, J.L. Johnson, E.A. Patten, K. Kasai, P.M. Goetz, S.M. Johnson, Molecular beam epitaxial growth and performance of HgCdTe-based simultaneous-mode two-color detectors, J. Electron. Mater. 27 (1998) 747–751.

[58] M.B. Reine, A. Hairston, P. O'Dette, S.P. Tobin, F.T.J. Smith, B.L. Musicant, P. Mitra, F.C. Case, Simultaneous MW/LW dual-band MOCVD HgCdTe 64×64 FPAs, Proc. SPIE 3379 (1998) 200–212.

[59] S.M. Johnson, J.L. Johnson, W.J. Hamilton, D.B. Leonard, T.A. Strand, A.E. Patten, J.M. Peterson, J.H. Durham, V.K. Randall, T.J. de Lyon, J.E. Jensen, M.D. Gorwitz, HgCdZnTe quaternary materials for lattice-matched two-color detectors, J. Electron. Mater. 29 (2000) 680–686.

[60] P. Ferret, J.P. Zanatta, R. Hamelin, S. Cremer, A. Million, M. Wolny, G. Destefanis, Status of the MBE technology at Leti LIR for the manufacturing of HgCdTe focal plane arrays, J. Electron. Mater. 29 (2000) 641–647.

[61] W.E. Tennant, M. Thomas, L.J. Kozlowski, W.V. McLevige, D.D. Edwall, M. Zandian, K. Spariosu, G. Hildebrandt, V. Gil, P. Ely, M. Muzilla, A. Stoltz, J.H. Dinan, A novel simultaneous unipolar multispectral integrated technology approach for HgCdTe IR detectors and focal plane arrays, J. Electron. Mater. 30 (2001) 590–594.

[62] W.A. Beck, T.S. Faska, Current status of quantum well focal plane arrays, Proc. SPIE 2744 (1996) 193–206.

[63] T. Whitaker, Sanders' QWIPs detect two color at once, Compd. Semicond. 5 (7) (1999) 48–51.

[64] S.D. Gunapala, S.V. Bandara, A. Sigh, J.K. Liu, S.B. Rafol, E.M. Luong, J.M. Mumolo, N.Q. Tran, J.D. Vincent, C.A. Shott, J. Long, P.D. Le Van, 8–9 and 14–15 μm two-color 640×486 quantum well infrared photodetector (QWIP) focal plane array camera, Proc. SPIE 3698 (1999) 687–697.

[65] P. Bois, E. Costard, X. Marcadet, E. Herniou, Development of quantum well infrared photodetectors in France, Infrared Phys. Technol. 42 (2001) 291–300.

[66] M. Sundaram, S.C. Wang, M.F. Taylor, A. Reisinger, G.L. Milne, K.B. Reiff, R.E. Rose, R.R. Martin, Infrared Phys. Technol. 42 (2001) 301–308.

[67] M.Z. Tidrow, J.C. Chiang, S.S. Li, K. Bacher, A high strain two-stack two-color quantum well infrared photodetector, Appl. Phys. Lett. 70 (1997) 859–861.

[68] C.T. Elliott, Photoconductive and non-equilibrium devices in HgCdTe and related alloys, in: P. Capper, C.T. Elliott (Eds.), Infrared Detectors and Emitters: Materials and Devices, Kluwer Academic Publishers, Boston, 2000, pp. 279–312.

[69] J. Piotrowski, M. Grudzień, Z. Nowak, Z. Orman, J. Pawluczyk, M. Romanis, W. Gawron, Uncooled photovoltaic $Hg_{1-x}Cd_xTe$ LWIR detectors, Proc. SPIE 4130 (2000) 175–184.

[70] T. Perazzo, M. Mao, O. Kwon, A. Majumdar, J.B. Varesi, P. Norton, Infrared vision using uncooled micro-optomechanical camera, Appl. Phys. Lett. 74 (2001) 3567–3569.